Adv Comput Math (2008) 29:179–206
DOI 10.1007/s10444-007-9050-7

The spectral method and numerical continuation algorithm for the von Kármán problem with postbuckling behaviour of solutions

Aliki D. Muradova

Received: 5 June 2005 / Accepted: 28 January 2007 /
Published online: 25 May 2007

Abstract In this paper a spectral method and a numerical continuation algorithm for solving eigenvalue problems for the rectangular von Kármán plate with different boundary conditions (simply supported, partially or totally clamped) and physical parameters are introduced. The solution of these problems has a postbuckling behaviour. The spectral method is based on a variational principle (Galerkin's approach) with a choice of global basis functions which are combinations of trigonometric functions. Convergence results of this method are proved and the rate of convergence is estimated. The discretized nonlinear model is treated by Newton's iterative scheme and numerical continuation. Branches of eigenfunctions found by the algorithm are traced. Numerical results of solving the problems for polygonal and ferroconcrete plates are presented.

Keywords Nonlinear partial differential equations · Von Kármán plates · Eigenvalue problems · Bifurcation phenomenon · Spectral method · Iterative scheme · Numerical continuation algorithm

Mathematics Subject Classifications (2000) 74K20 · 35B32 · 65N25 · 65N35 · 65T40 · 65F10

Communicated by A. Zhou.

A. D. Muradova (✉)
The Mathematical Sciences Institute, Buil. No 27, The Australian National University, 0200, ACT, Canberra, Australia
e-mail: Aliki.Muradova@maths.anu.edu.au

Present address:
Dept. of Mineral Resources and Engineering, The Technical University of Crete, Chania 73100, Crete, Greece
e-mail: aliki@mred.tuc.gr

1 Introduction

We study eigenvalue problems for the von Kármán plate with postbuckling behaviour of solution. The plate is supposed to be simply supported, partially or totally clamped. A bifurcation phenomenon is investigated for these cases.

The von Kármán equations have been explored by many authors ([4–10, 12–16] and others). The existing techniques for treating the mechanical model are based on finite elements and finite difference approximations. The discrete problems which are obtained after discretization, are solved by a Newton-GMRES algorithm in the context of sophisticated numerical continuation of Allgower and Georg [3].

The postbuckling behaviour of the solution depends on the boundary conditions. In some cases, for instance for the totally clamped plates, it can be quite complicated and investigations in this situation are interesting from both the physical and mathematical point of view. The most noteworthy feature of studies of the postbuckling behaviour is so-called mode jumping. This implies nonstability of the primary solution branches through further bifurcation. This phenomenon was investigated extensively by Holder, Schaeffer and Golubitsky ([12, 15]). Later their theoretical results for the partially clamped plate, subjected to compression along its two sides were verified numerically by Chien, Gong and Mei in [6].

A topology of bifurcation diagrams for the von Kármán problem for a totally clamped polygonal plate (with all physical parameters equal unity) is analyzed by the Newton-GMRES algorithm in a recent paper of Dossou and Pierre [10] and in Dossou's thesis [9].

In the present paper we introduce a spectral method for solving the eigenvalue problems for the rectangular von Kármán plate with different physical parameters. The spectral method is based on a variational principle (Galerkin's approach) with a choice of global basis functions which span the whole domain.

A major advantage of the spectral method over the finite differences or finite elements is its high convergence order. The rate of decrease of the error with increasing a number of the global functions, depends on the smoothness of the solution being approximated. A few partial sums of the series are required to obtain the desired accuracy.

The proposed method guarantees high accuracy and it allows us easily to compute eigenfunctions. We use partial sums of the Fourier series to expand solutions and analyze the error of approximation. The Fourier coefficients are good guides for following branches of the solutions and the chosen trigonometric functions reflect the shape of the eigenfunctions. Convergence results are proved and the rate of convergence is estimated.

The discrete nonlinear model, which is obtained after the use of the spectral method, is solved by a combination of the Newton and numerical continuation algorithms.

There are several techniques for solving the nonlinear system of algebraic equations which is obtained after discretization of the mechanical model. For instance, in [9] and [10] a perturbation in the equations is used. From the trivial branch the authors follow the perturbed branch until it is sufficiently close to the non perturbed branch. Then the perturbation is canceled and with the Newton method the first point on the non perturbed branch is found. When the first point is obtained, some numerical continuation method is applied to trace the branch of the solution. In

particular, the predictor-corrector (Euler–Newton) continuation algorithm ([13]) is exploited. The predictor-corrector method, combined with block GMRES (BGMRES) is implemented by Chien, Chang and Mei in [5] to trace solution curves of the associated discrete problem.

In this paper the perturbation is not used. The first point of the solution curve is found by the Newton iterations with the initial approximation (starting guess) chosen according to the properties of the Fourier coefficients in the expansion of the solution (Steps 2, 3 in the algorithm of Section 5.2). When the first point is computed, the numerical continuation with a scalar detector (Steps 4–7 in the algorithm and paragraph 3 of Section 5.2) is applied.

The paper is structured as follows. In Section 2 the mechanical model is formulated. We consider different states of the plate and set up conditions for existence of multisolutions. Section 3 is devoted to the spectral method. As is known, a key step in any variational approach is the selection of a coordinate system of trial (basis) functions. We introduce global basis functions for different boundary conditions. Then the convergence results for the method are demonstrated. In Section 4 we compute the primary bifurcation points by solving the linearized problem. The rule of separation and the Galerkin method are applied. In Section 5 the iterative scheme based on the Newton iterations and numerical continuation algorithm is constructed. Section 6 illustrates numerical examples of solving the given problems for the plate with different sizes and properties.

2 The nonlinear mechanical model and boundary conditions

The nonlinear equations describing the bending and stretching of a thin rectangular plate with buckling are

$$\begin{aligned} D\Delta^2 w &= 2h_0[w,\psi] + \lambda[\theta, w], \quad (x, y) \in G, \\ \Delta^2 \psi &= -\frac{E}{2}[w, w], \end{aligned} \tag{1}$$

where $G = (0, l_1) \times (0, l_2)$ (l_1 and l_2 are lengths of sides of the plate) is the shape of the plate, $[w, \psi] = \frac{\partial^2 w}{\partial x^2}\frac{\partial^2 \psi}{\partial y^2} + \frac{\partial^2 \psi}{\partial x^2}\frac{\partial^2 w}{\partial y^2} - 2\frac{\partial^2 w}{\partial x \partial y}\frac{\partial^2 \psi}{\partial x \partial y}$, $w(x, y)$ denotes the deflection, $\psi(x, y)$ is the Airy stress potential, $\theta(x, y)$ is a regular function defined on G, with values which depend on the portion of the boundary subjected to compression, λ is the intensity of this compression, $D = \frac{2Eh_0^3}{3(1-\nu^2)}$ is the cylindrical rigidity, E is Young's modulus, $2h_0$ is the thickness of the plate, and ν is Poisson's ratio.[1]

Regarding to the regularity of the solution we require that w, ψ belong to the Sobolev space $W^{2,2}(G)$ ([1]). Thus, we are looking for a solution which, according to the standard definition of the Sobolev space, has up to the second order partial derivatives in weak (distributional) sense and this solution with its derivatives

[1] In the equations (1) the loading function $f = 0$. The proposed techniques are also applicable to the case when $f \neq 0$. In this case we consider δf, where $\delta \in [0, 1]$ might be used as an incremental loading parameter ([8]).

belongs to L_2 space. This assumption is used in Section 3.2 and 3.3 to prove Lemmas 3.1, 3.2 and Theorem 3.1.

If the plate is compressed on all sides then

$$\theta(x, y) = -\frac{1}{2}(x^2 + y^2)\,.$$

Compression on two sides only implies, without loss of generality,

$$\theta(x, y) = -\frac{1}{2}y^2\,.$$

Then we can write down (1) as

$$\begin{aligned} D\Delta^2 w &= 2h_0[w, \psi] - \lambda L w \quad (x, y) \in G\,, \\ \Delta^2 \psi &= -\frac{E}{2}[w, w]\,, \end{aligned} \tag{2}$$

where the operator L is Δ or $\frac{\partial^2}{\partial x^2}$ according to the definition of θ function.

According to the results of [8], if $\lambda \le \lambda_1$, where λ_1 is the first eigenvalue of the linearized equation

$$D\Delta^2 w + \lambda L w = 0 \quad (x, y) \in G\,, \tag{3}$$

then (2) has a unique trivial solution. Otherwise ($\lambda > \lambda_1$) (2) has at least three solutions (w, ψ), $(-w, \psi)$, $(w \neq 0, \psi \neq 0)$ and $(0, 0)$.

When the plate is simply supported the classical boundary conditions are

$$\begin{aligned} &(a) \quad w = 0\,, \quad \Delta w = 0 \quad (x, y) \in \partial G\,, \\ &(b) \quad \psi = 0\,, \quad \Delta \psi = 0 \quad (x, y) \in \partial G. \end{aligned} \tag{4}$$

A more appropriate condition in the physical sense for the stress function ([15]) is

$$\frac{\partial \psi}{\partial n} = \frac{\partial}{\partial n}\Delta\psi = 0 \quad (x, y) \in \partial G\,. \tag{5}$$

The simply supported boundary conditions (4) are convenient from the mathematical point of view but are notoriously difficult to achieve in experiments. The most accurate description are partially clamped or fully clamped boundary conditions.

The partially clamped plate denotes, e.g.,

$$w = \begin{cases} \dfrac{\partial w}{\partial n} = 0\,, & x = 0, l_1\,, \\ \Delta w = 0\,, & y = 0, l_2 \end{cases} \tag{6}$$

and the Airy stress function ψ satisfies (4b) or (5). In (5) and (6) $\frac{\partial}{\partial n}$ denotes the operator of the normal derivative. The conditions (6), (4b) and (6), (5) correspond to the clamped sides $x = 0, l_1$ and simply supported ends $y = 0, l_2$. Holder and Schaeffer in [12] considered (6) when the plate is compressed only on the clamped sides i.e., $L = \partial^2/\partial x^2$. This situation was also investigated numerically by Chien, Gong and Mei in [6], Chien, Chang and Mei in [5] and others.

The most realistic (totally clamped) boundary conditions are

$$w = \frac{\partial w}{\partial n} = 0 \quad (x, y) \in \partial G\,,$$
$$\psi = \frac{\partial \psi}{\partial n} = 0 \quad (x, y) \in \partial G\,. \tag{7}$$

3 The spectral method

3.1 Coordinate systems

In order to give systems of global coordinate functions we use combinations of trigonometric functions. The solution of (2) is expanded as partial sums of the double Fourier series:

$$W_N(x, y) = \sum_{i,j=1}^{N} w_N^{ij}\omega_{ij}(x, y), \quad \Psi_N(x, y) = \sum_{i,j=1}^{N} \psi_N^{ij}\varphi_{ij}(x, y)\,, \tag{8}$$

where ω_{ij} and φ_{ij} are global basis functions which are chosen to match the boundary conditions, and N is a natural number. A coordinate system $\{\omega_{ij}\}_{i,j=1}^{N}$ in the Sobolev space $W^{2,2}(G)$ must satisfy the following criteria:

1. $\{\omega_{ij}\}_{i,j=1}^{N} \in W^{2,2}(G)$;
2. The elements of $\{\omega_{ij}\}_{i,j=1}^{N}$ are linearly independent;
3. $\{\omega_{ij}\}_{i,j=1}^{N}$ is complete in the Sobolev space $W^{2,2}(G)$.

For the simply supported plate (4a), (4b) or (5) suitable bases are eigenfunctions of the Laplacian under the Dirichlet or Neumann conditions, respectively, i.e.,

$$\omega_{ij}(x, y) = \varphi_{ij}(x, y) = \frac{2}{\sqrt{l_1 l_2}} \sin\left(\frac{i}{l_1}\pi x\right) \sin\left(\frac{j}{l_2}\pi y\right) \tag{9}$$

or

$$\varphi_{ij}(x, y) = \frac{2}{\sqrt{l_1 l_2}} \cos\left(\frac{i}{l_1}\pi x\right) \cos\left(\frac{j}{l_2}\pi y\right) \quad i, j = 1, 2, \ldots, N. \tag{10}$$

For the partially clamped plate (6) we introduce a new basis

$$\omega_{ij}(x, y) = \chi \cos\left(\frac{i}{l_1}\pi x\right) \sqrt{\frac{2}{l_2}} \sin\left(\frac{j}{l_2}\pi y\right)\,, \tag{11}$$

where $\chi \cos\left(\frac{i}{l}\pi x\right)$ are the first order divided differences from the cosine functions, i.e.,

$$\chi \cos\left(\frac{i}{l}\pi x\right) = \sqrt{\frac{2}{l}} \left(\cos\left(\frac{i+1}{l}\pi x\right) - \cos\left(\frac{i-1}{l}\pi x\right)\right) \tag{12}$$

and the functions $\varphi_{ij}(x, y)$ are determined as before. The system $\{\omega_{ij}\}_{i=1}^{N}$ defined by (11) is a system of linear independent elements for arbitrary N which is complete in the Sobolev space $W^{2,2}(G)$ and satisfies the boundary conditions (6) so that Criteria

1,2,3 hold. Criterion 2 can be verified by computing the Gram determinant of the elements ω_{ij}. Criteria 1,3 are true by virtue of the definition of $\chi\cos\left(\frac{i}{l}\pi x\right)$.

Note, that the difference expressions $\cos\left(\frac{i}{l}\pi x\right)-\cos\left(\frac{i+2}{l}\pi x\right)$ are eigenfunctions of the ordinary differential equation which is obtained after the use of the rule of separation to $\Delta^2 w+\lambda w_{xx}=0$ (e.g. [5, 12, 15]).

When we have the totally clamped plate (7) the previously introduced functions (12) are applied, i.e.:

$$\omega_{ij}(x,y)=\varphi_{ij}(x,y)=\chi\cos\left(\frac{i}{l_1}\pi x\right)\chi\cos\left(\frac{j}{l_2}\pi y\right). \tag{13}$$

Obviously they satisfy (7).

3.2 Discretization

Let us consider the scalar product in L_2, i.e.,

$$\langle u,v\rangle=\int_G uvdG.$$

Applying Galerkin's projections to (2) yields (see (8))

$$\begin{aligned} D\langle\Delta^2 W_N,\omega_{mn}\rangle &= 2h_0\langle[W_N,\Psi_N],\omega_{mn}\rangle-\lambda\langle LW_N,\omega_{mn}\rangle,\\ \langle\Delta^2\Psi_N,\varphi_{mn}\rangle &= -\tfrac{E}{2}\langle[W_N,W_N],\varphi_{mn}\rangle, \quad m,n=1,2,\ldots,N. \end{aligned}$$

Hence we get a system of nonlinear algebraic equations which in the matrix form is

$$\begin{aligned} \mathbf{K_1 w_N} &= \mathbf{A_{1,N}}(\mathbf{w_N},\boldsymbol{\psi_N})+\lambda\mathbf{B w_N},\\ \mathbf{K_2}\boldsymbol{\psi_N} &= \mathbf{A_{2,N}}(\mathbf{w_N},\mathbf{w_N}), \end{aligned} \tag{14}$$

where $\mathbf{w_N}=\left(w_N^{11},\ldots,w_N^{1N},w_N^{21},\ldots,w_N^{2N},\ldots,\ w_N^{N1},\ldots,w_N^{NN}\right)^T$ and $\boldsymbol{\psi_N}=\left(\psi_N^{11},\ldots,\psi_N^{1N},\psi_N^{21},\ldots,\psi_N^{2N},\ldots,\psi_N^{N1},\ldots,\psi_N^{NN}\right)^T$ are vectors with components which are the Fourier coefficients in (8) grouped by rows, $\mathbf{K_1}$, $\mathbf{K_2}$ and $\mathbf{B}$ are matrices with dimension $N^2\times N^2$, arising from the approximations of the biharmonic operators and the operator L, respectively. Further, $\mathbf{A_{1,N}}(\mathbf{w_N},\boldsymbol{\psi_N})$ and $\mathbf{A_{2,N}}(\mathbf{w_N},\mathbf{w_N})$ are vectors with dimension N^2 and components which are nonlinear quadratic forms arising from the second order nonlinear geometric terms, according to the assumptions of the von Kármán plate theory.

The system (14) can be written down as

$$\begin{aligned} (\mathbf{K_1 w_N})_{mn} &= (\mathbf{A_{1,N}}(\mathbf{w_N},\boldsymbol{\psi_N}))_{mn}+\lambda(\mathbf{B w_N})_{mn},\\ (\mathbf{K_2}\boldsymbol{\psi_N})_{mn} &= (\mathbf{A_{2,N}}(\mathbf{w_N},\mathbf{w_N}))_{mn}, \quad m,n=1,2,\ldots,N. \end{aligned} \tag{15}$$

Due to (4) and (5) we have the simplest form for $(\mathbf{K_1 w_N})_{mn}$ and $(\mathbf{K_2}\boldsymbol{\psi_N})_{mn}$:

$$(\mathbf{K_1 w_N})_{mn}=D\lambda_{mn}^2 w_N^{mn}, \quad (\mathbf{K}_2\boldsymbol{\psi_N})_{mn}=\lambda_{mn}^2\psi_N^{mn} \tag{16}$$

and

$$(\mathbf{B}\mathbf{w}_\mathbf{N})_{mn} = \begin{cases} \lambda_{mn} w_N^{mn}, & L = \Delta, \\ \pi^2 \left(\frac{m}{l_1}\right)^2 w_N^{mn}, & L = \frac{\partial^2}{\partial x^2}, \end{cases} \tag{17}$$

where $\lambda_{mn} = \pi^2 \left(\left(\frac{m}{l_1}\right)^2 + \left(\frac{n}{l_2}\right)^2 \right)$ are eigenvalues of the Laplacian.

When the partially clamped conditions hold then we have the tri-point approximation, namely

$$(\mathbf{K_1}\mathbf{w}_\mathbf{N})_{mn} = -q_{m-1,n} w_N^{m-2,n} + (q_{m+1,n} + q_{m-1,n}) w_N^{mn} - q_{m+1,n} w_N^{m+2,n}, \tag{18}$$

$(\mathbf{K_2}\mathbf{w}_\mathbf{N})_{mn}$ is defined as before and

$$(\mathbf{B}\mathbf{w}_\mathbf{N})_{mn} = -b_{m-1,n} w_N^{m-2,n} + (b_{m+1,n} + b_{m-1,n}) w_N^{mn} - b_{m+1,n} w_N^{m+2,n}, \tag{19}$$

where $q_{mn} = D\left(\lambda_{mn}^2 + \left(\frac{\pi n}{l_2}\right)^4 \delta_{m,1}\right)$, $b_{mn} = \begin{cases} \lambda_{mn} + \left(\frac{\pi m}{l_1}\right)^2 \delta_{m,1}, & L = \Delta, \\ \pi^2 \left(\frac{m}{l_1}\right)^2, & L = \frac{\partial^2}{\partial x^2} \end{cases}$ and

$\delta_{m,1} = \begin{cases} 1, & m = 1, \\ 0, & m \neq 1. \end{cases}$

For the totally clamped plate we obtain the nine-point stencil, i.e.,

$$\begin{aligned} (\mathbf{K_1}\mathbf{w}_\mathbf{N})_{mn} = {} & q_{mn}^1 w_N^{m-2,n-2} + q_{mn}^2 w_N^{m-2,n} + q_{mn}^3 w_N^{m-2,n+2} \\ & + q_{mn}^4 w_N^{m,n-2} + q_{mn}^5 w_N^{mn} + q_{mn}^6 w_N^{m,n+2} \\ & + q_{mn}^7 w_N^{m+2,n-2} + q_{mn}^8 w_N^{m+2,n} + q_{mn}^9 w_N^{m+2,n+2}, \end{aligned} \tag{20}$$

$(\mathbf{K_2}\boldsymbol{\psi}_\boldsymbol{N})_{mn}$ is defined similarly, just putting $D = 1$ and for $(\mathbf{B}\mathbf{w}_\mathbf{N})_{mn}$ we have

$$\begin{aligned} (\mathbf{B}\mathbf{w}_\mathbf{N})_{mn} = {} & b_{mn}^1 w_N^{m-2,n-2} + b_{mn}^2 w_N^{m-2,n} + b_{mn}^3 w_N^{m-2,n+2} \\ & + b_{mn}^4 w_N^{m,n-2} + b_{mn}^5 w_N^{mn} + b_{mn}^6 w_N^{m,n+2} \\ & + b_{mn}^7 w_N^{m+2,n-2} + b_{mn}^8 w_N^{m+2,n} + b_{mn}^9 w_N^{m+2,n+2}. \end{aligned} \tag{21}$$

Here q_{mn}^i and b_{mn}^i, $i = 1, 2, \ldots, 9$ are coefficients which are defined the same as q_{mn} and b_{mn}, respectively.

The nonlinear forms $(\mathbf{A_{1,N}}(\mathbf{w_N}, \boldsymbol{\psi_N}))_{mn}$ and $(\mathbf{A_{2,N}}(\mathbf{w_N}, \mathbf{w_N}))_{mn}$ in (15) are determined as:

$$(\mathbf{A_{1,N}}(\mathbf{w_N}, \boldsymbol{\psi_N}))_{mn} = 2h_0 \sum_{i,j,k,l=1}^{N} w_N^{ij} \psi_N^{kl} a_1(i,k,m,j,l,n),$$

$$(\mathbf{A_{2,N}}(\mathbf{w_N}, \mathbf{w_N}))_{mn} = -\frac{E}{2} \sum_{i,j,k,l=1}^{N} w_N^{ij} w_N^{kl} a_2(i,k,m,j,l,n),$$

where a_1 and a_2 are functions of discrete variables, which are bounded with respect to m and n. For example, for the simply supported plate (4):

$$a_1 = a_2 = \frac{\pi^2}{2(l_1 l_2)^{5/2}} \left[\left(a_{ikm}^1 a_{jln}^1 + a_{ikm}^2 a_{jln}^2\right)(il - jk)^2 - \left(a_{ikm}^1 a_{jln}^2 + a_{ikm}^2 a_{jln}^1\right)(il + jk)^2 \right],$$

where $a^1_{ikm} = \frac{\cos\pi(m+i+k)-1}{m+i+k} + \frac{\cos\pi(m-i-k)-1}{m-i-k}$, $a^2_{ikm} = \frac{\cos\pi(m+i-k)-1}{m+i-k} + \frac{\cos\pi(m-i+k)-1}{m-i+k}$. For the other cases the functions a_1 and a_2 are defined similarly.

3.3 Convergence

Let us now analyze the system (15). The Fourier series representation of the solution of (2) is

$$W(x, y) = \sum_{i,j=1}^{\infty} w^{ij}\omega_{ij}(x, y), \quad \Psi(x, y) = \sum_{i,j=1}^{\infty} \psi^{ij}\varphi_{ij}(x, y) \tag{22}$$

(we have dropped the index N for the exact solution). Then we can say that (15) is a truncated system of the infinite one:

$$\begin{aligned} (\mathbf{K_1 w})_{mn} &= (\mathbf{A_1}(\mathbf{w}, \boldsymbol{\psi}))_{mn} + \lambda(\mathbf{B}w)_{mn}\,, \\ (\mathbf{K_2}\boldsymbol{\psi})_{mn} &= (\mathbf{A_2}(\mathbf{w}, \mathbf{w}))_{mn}\,, \quad m, n = 1, 2, \ldots, \infty\,. \end{aligned} \tag{23}$$

Here it has been assumed $\mathbf{A}_{\mathbf{1},\infty} \equiv \mathbf{A_1}$, $\mathbf{A}_{\mathbf{2},\infty} \equiv \mathbf{A_2}$. The following lemma estimates the Fourier coefficients in (22).

Lemma 3.1 *For the Fourier coefficients w^{mn}, ψ^{mn} in the expansions (22) of the functions $W(x, y)$ and $\Psi(x, y)$, for fixed λ, the following estimates hold:*

$$w^{mn} = O\left((mn)^{-1}(m^2+n^2)^{-2}\right), \quad \psi^{mn} = O\left((mn)^{-1}(m^2+n^2)^{-2}\right). \tag{24}$$

Proof Since the series (22) converge then w^{mn}, $\psi^{mn} \to 0$ when $m, n \to \infty$. Let us consider (16) and (17) ($L = \Delta$). Then (23) will have the form

$$\begin{aligned} D\lambda^2_{mn} w^{mn} &= (\mathbf{A_1}(\mathbf{w}, \boldsymbol{\psi}))_{mn} + \lambda\lambda_{mn} w^{mn}, \\ \lambda^2_{mn}\psi^{mn} &= (\mathbf{A_2}(\mathbf{w}, \mathbf{w}))_{mn}\,, \quad m, n = 1, 2, \ldots, \infty\,. \end{aligned} \tag{25}$$

The necessary estimates (24) follow from (25) in virtue of λ is fixed and the definitions of λ_{mn}, a_1 and a_2.

Analogously we can obtain the estimates when (17) ($L = \partial^2/\partial x^2$) holds and for the other boundary conditions (see (18–21)). □

Let us now introduce the notations

$$\begin{aligned} &\varepsilon^{mn}_{1,N} = w^{mn} - w^{mn}_N,\ \varepsilon^{mn}_{2,N} = \psi^{mn} - \psi^{mn}_N \quad \text{for} \quad m, n = 1, 2, \ldots, N; \\ &\varepsilon^{mn}_{1,N} = w^{mn},\ \varepsilon^{mn}_{2,N} = \psi^{mn} \qquad\qquad \text{for} \quad m, n = N+1, N+2, \ldots, \infty; \\ &\quad m = 1, 2, \ldots, \infty,\ n = N+1, N+2, \ldots, \infty \quad \text{and} \\ &\quad m = N+1, N+2, \ldots, \infty,\ n = 1, 2, \ldots, \infty. \end{aligned} \tag{26}$$

Here $\{\boldsymbol{\varepsilon_{1,N}}, \boldsymbol{\varepsilon_{2,N}}\}$ denote the error of the truncated system with respect to the infinite one.

Lemma 3.2 *A sequence* $\{w^{mn}_N, \psi^{mn}_N,\ m, n = 1, 2, \ldots, \infty$ ($w^{mn}_N = \psi^{mn}_N = 0$, *for* $m = 1, 2, \ldots, \infty,\ n = N+1, N+2, \ldots, \infty; m = N+1, N+2, \ldots, \infty,\ n = 1, 2, \ldots, \infty$

and $m, n = N+1, N+2, \ldots, \infty)\}$, *where* $\{w_N^{mn}, \psi_N^{mn},\ m, n = 1, 2, \ldots, N\}$ *are eigenfunctions of* (15), *for fixed* λ, *converges to the sequence* $\{w^{mn},\ \psi^{mn},\ m, n = 1, 2, \ldots, \infty\}$, *satisfying* (23). *Moreover,*

$$\left|\varepsilon_{p,N}^{mn}\right| < C_0 (mn)^{-1} (m^2 + n^2)^{-2} N^{-4} \ln N, \quad p = 1, 2, \tag{27}$$

where C_0 *is a positive constant depending on the physical parameters of the plate.*

Proof The system (23) can be written down in the following form:

$$\begin{aligned} (\mathbf{K_1 w})_{mn} &= (\mathbf{A_{1,N}}(\mathbf{w}, \boldsymbol{\psi}))_{mn} + (\mathbf{R_{1,N}}(\mathbf{w}, \boldsymbol{\psi}))_{mn} + \lambda (\mathbf{B w})_{mn}, \\ (\mathbf{K_2 \boldsymbol{\psi}})_{mn} &= (\mathbf{A_{2,N}}(\mathbf{w}, \mathbf{w}))_{mn} + (\mathbf{R_{2,N}}(\mathbf{w}, \mathbf{w}))_{mn}, \\ & \qquad m, n = 1, 2, \ldots, \infty, \end{aligned} \tag{28}$$

where

$$\begin{aligned} (\mathbf{R_{1,N}}(\mathbf{w}, \boldsymbol{\psi}))_{mn} = & \sum_{i,j,k,l=N+1}^{\infty} w^{ij} \psi^{kl} a_1(i, k, m, j, l, n) \\ & + \sum_{i,j,k=N+1}^{\infty} \sum_{l=1}^{N} w^{ij} \psi^{kl} a_1(i, k, m, j, l, n) + \ldots \\ & + \sum_{i,j=N+1}^{\infty} \sum_{k,l=1}^{N} w^{ij} \psi^{kl} a_1(i, k, m, j, l, n) + \ldots \\ & + \sum_{i=N+1}^{\infty} \sum_{j,k,l=1}^{N} w^{ij} \psi^{kl} a_1(i, k, m, j, l, n) + \ldots \end{aligned}$$

and $(\mathbf{R_{2,N}}(\mathbf{w}, \boldsymbol{\psi}))_{mn}$ is determined analogously.

By Lemma 3.1 when $N \to \infty$

$$\begin{aligned} \sum_{i=1}^{N} \sum_{j=N+1}^{\infty} w^{ij} &\le c_1 \sum_{j=N+1}^{\infty} \sum_{i=1}^{N} \frac{1}{ij(i^2 + j^2)^2} \\ &= c_1 \sum_{j=N+1}^{\infty} \frac{1}{j} \sum_{i=1}^{N} \left(\frac{1}{j^4 i} - \frac{i}{j^2 (i^2 + j^2)^2} - \frac{i}{j^4 (i^2 + j^2)} \right) \\ &< c_1 \sum_{j=N+1}^{\infty} \frac{1}{j} \sum_{i=1}^{N} \left(\frac{1}{j^4 i} + \frac{i}{j^2 (i^2 + j^2)^2} + \frac{i}{j^4 (i^2 + j^2)} \right) \end{aligned}$$

$$< c_1 \sum_{j=N+1}^{\infty} \frac{1}{j} \sum_{i=1}^{N} \left(\frac{1}{j^4 i} + \frac{i}{2j^4 i^2} + \frac{i}{j^4 i^2} \right)$$

$$< c_1 \sum_{j=N+1}^{\infty} \frac{1}{j^5} \sum_{i=1}^{N} \left(\frac{2}{i} + \frac{1}{2i} \right)$$

$$< 2.5 c_1 \frac{\ln N}{N^4}, \tag{29}$$

$$\sum_{i=1}^{N} \sum_{j=1}^{N} w^{ij} < c_1 \sum_{j=1}^{N} \sum_{i=1}^{N} \frac{1}{ij(i^2 + j^2)^2}$$

$$= c_1 \sum_{j=1}^{N} \frac{1}{j^3} \sum_{i=1}^{N} \left(\frac{1}{i(i^2 + j^2)} - \frac{i}{(i^2 + j^2)^2} \right)$$

$$< c_1 \sum_{j=1}^{N} \frac{1}{j^3} \sum_{i=1}^{N} \left(\frac{1}{i(i^2 + j^2)} + \frac{i}{(i^2 + j^2)^2} \right)$$

$$< c_1 \sum_{j=1}^{N} \frac{1}{j^3} \sum_{i=1}^{N} \frac{2}{i^3}$$

$$< 8 c_1, \tag{30}$$

$$\sum_{i=N+1}^{\infty} \sum_{j=N+1}^{\infty} w^{ij} < c_1 \sum_{j=N+1}^{\infty} \sum_{i=N+1}^{\infty} \frac{1}{ij(i^2 + j^2)^2}$$

$$= c_1 \sum_{j=N+1}^{\infty} \frac{1}{j^3} \sum_{i=N+1}^{\infty} \left(\frac{1}{i(i^2 + j^2)} - \frac{i}{(i^2 + j^2)^2} \right)$$

$$< c_1 \sum_{j=N+1}^{\infty} \frac{1}{j^3} \sum_{i=N+1}^{\infty} \left(\frac{1}{i(i^2 + j^2)} + \frac{i}{(i^2 + j^2)^2} \right)$$

$$< c_1 \sum_{j=N+1}^{\infty} \frac{1}{j^3} \sum_{i=N+1}^{\infty} \frac{2}{i^3}$$

$$< \frac{2c_1}{N^4}, \quad (c_1 = const > 0). \tag{31}$$

Then in accordance with Lemma 3.1, the inequalities (29–31) and the definitions of a_1 and a_2 for $R_{1,N}$ we obtain

$$|(\mathbf{R_{1,N}}(\mathbf{w}, \boldsymbol{\psi}))_{mn}| < c \frac{\ln N}{N^4}, \quad (c = const > 0). \tag{32}$$

The same estimate we obtain for $(\mathbf{R_{2,N}}(\mathbf{w}, \boldsymbol{\psi}))_{mn}$.

Subtracting (15) from (28), respectively and using the notations (26) we have

$$\begin{aligned}((\mathbf{K_1}-\lambda\mathbf{B})\boldsymbol{\varepsilon_{1,N}})_{mn} &= (\mathbf{A_{1,N}}(\boldsymbol{\varepsilon_{1,N}},\boldsymbol{\varepsilon_{2,N}}))_{mn}+(\mathbf{A_{1,N}}(\mathbf{w},\boldsymbol{\varepsilon_{2,N}}))_{mn}\\ &\quad+(\mathbf{A_{1,N}}(\boldsymbol{\varepsilon_{1,N}},\boldsymbol{\psi}))_{mn}+(\mathbf{R_{1,N}}(\mathbf{w},\boldsymbol{\psi}))_{mn},\\ (\mathbf{K_2}\boldsymbol{\varepsilon_{2,N}})_{mn} &= (\mathbf{A_{2,N}}(\boldsymbol{\varepsilon_{1,N}},\boldsymbol{\varepsilon_{1,N}}))_{mn}+2(\mathbf{A_{2,N}}(\mathbf{w},\boldsymbol{\varepsilon_{1,N}}))_{mn}\\ &\quad+(\mathbf{R_{2,N}}(\mathbf{w},\mathbf{w}))_{mn},\quad m,n=1,2,\ldots,\infty. \end{aligned}\tag{33}$$

We have shown that $(\mathbf{R_{1,N}}(\mathbf{w},\boldsymbol{\psi}))_{mn}\to 0$ and $(\mathbf{R_{2,N}}(\mathbf{w},\mathbf{w}))_{mn}\to 0$ when $N\to\infty$. This implies $\mathbf{A_{p,N}}\sim\mathbf{A_p}$. Consequently $\boldsymbol{\varepsilon_{p,N}}\to 0$ when $N\to\infty$.

By virtue of the definitions of $\mathbf{K_p}$, $\mathbf{B}$, $\mathbf{A_{p,N}}$ (see (16–21)) and (32) from (33) we obtain the estimates (27) for $\varepsilon^{mn}_{p,N}$. □

Now let us prove a theorem which allows for the evaluation of the approximate solution $W_N(x,y)$, $\Psi_N(x,y)$.

Assume $\delta_{1,N}(x,y)=W(x,y)-W_N(x,y)$, $\delta_{2,N}(x,y)=\Psi(x,y)-\Psi_N(x,y)$ and $\|\delta\|=\max\limits_{(x,y)\in G}|\delta(x,y)|$.

Theorem 3.1 *For fixed λ the following inequalities hold:*

$$\|\delta_{p,N}\|<C\frac{\ln N}{N^4},\quad p=1,2,$$

where C is a positive constant depending on the physical parameters of the plate.

Proof Let us write down (22) in the following form:

$$\begin{aligned}W(x,y)&=\sum_{i,j=1}^{N}w^{ij}\omega_{ij}(x,y)+r_{1,N}(x,y),\\ \Psi(x,y)&=\sum_{i,j=1}^{N}\psi^{ij}\varphi_{ij}(x,y)+r_{2,N}(x,y),\end{aligned}\tag{34}$$

where

$$\begin{aligned}r_{1,N}(x,y)&=\sum_{i=1}^{N}\sum_{j=N+1}^{\infty}w^{ij}\omega_{ij}(x,y)+\sum_{i=N+1}^{\infty}\sum_{j=1}^{N}w^{ij}\omega_{ij}(x,y)\\ &\quad+\sum_{i=N+1}^{\infty}\sum_{j=N+1}^{\infty}w^{ij}\omega_{ij}(x,y),\end{aligned}\tag{35}$$

$$\begin{aligned}r_{2,N}(x,y)&=\sum_{i=1}^{N}\sum_{j=N+1}^{\infty}\psi^{ij}\varphi_{ij}(x,y)+\sum_{i=N+1}^{\infty}\sum_{j=1}^{N}\psi^{ij}\varphi_{ij}(x,y)\\ &\quad+\sum_{i=N+1}^{\infty}\sum_{j=N+1}^{\infty}\psi^{ij}\varphi_{ij}(x,y).\end{aligned}\tag{36}$$

Consider the first combination of the sums in (35). By virtue of Lemma 3.1, the definition of $\omega_{ij}(x, y)$ (see (9), (10), (11) and (13)) and (29) the following inequality holds.

$$\left|\sum_{i=1}^{N}\sum_{j=N+1}^{\infty} w^{ij}\omega_{ij}(x, y)\right| \leq \frac{8}{\sqrt{l_1 l_2}}\sum_{i=1}^{N}\sum_{j=N+1}^{\infty}|w^{ij}| < \frac{20}{\sqrt{l_1 l_2}}c_1\frac{\ln N}{N^4}.$$

Analogous evaluations are obtained for the second term in (35) and (36). For the last term in (35) and (36) in virtue of (31) we obtain

$$\left|\sum_{i=N+1}^{\infty}\sum_{j=N+1}^{\infty} w^{ij}\omega_{ij}(x, y)\right| \leq \frac{8}{\sqrt{l_1 l_2}}\sum_{i=N+1}^{\infty}\sum_{j=N+1}^{\infty}|w^{ij}| < \frac{16}{\sqrt{l_1 l_2}}\frac{c_1}{N^4}.$$

Finally we have

$$\|r_{p,N}\| < c_2\frac{\ln N}{N^4} \quad (c_2 = const > 0)\,.$$

Further according to (8) and (34):

$$\delta_{1,N}(x, y) = W(x, y) - W_N(x, y) = \sum_{i,j=1}^{N}\varepsilon_{1,N}^{ij}\omega_{ij}(x, y) + r_{1,N}(x, y),$$

$$\delta_{2,N}(x, y) = \Psi(x, y) - \Psi_N(x, y) = \sum_{i,j=1}^{N}\varepsilon_{2,N}^{ij}\varphi_{ij}(x, y) + r_{2,N}(x, y). \tag{37}$$

By Lemma 3.2 and the above obtained estimates for $r_{p,N}$ we deduce:

$$\|\delta_{p,N}\| \leq \frac{8}{\sqrt{l_1 l_2}}\sum_{k,l=1}^{N}|\varepsilon_{p,N}^{kl}| + \|r_{p,N}\| < C\frac{\ln N}{N^4}\,.$$

□

The established rate of convergence is obtained due to the regularity of the solution (Section 2, Paragraph 2) and the choice of the coordinate functions (Section 3.1) which are infinitely continuously differentiable.

4 The primary bifurcation points

Buckling loads λ, for which the solution bifurcates from the trivial one, correspond to eigenvalues of the appropriate linearized problem. The corresponding branches are primary branches and subsequent bifurcations from them are called secondary ones. We solve the linearized equation (3) to detect primary bifurcation points. For the simply supported plate (4) the eigenvalues of (3) will be

$$\overline{\lambda}_{mn} = \begin{cases} D\lambda_{mn}, & L = \Delta\,, \\ D\pi^2\left(\frac{m}{l_1} + \frac{l_1}{m}\left(\frac{n}{l_2}\right)^2\right)^2, & L = \frac{\partial^2}{\partial x^2}\,. \end{cases} \tag{38}$$

The corresponding eigenfunctions are $U_{mn}(x, y) = \frac{2}{\sqrt{l_1 l_2}} \sin(\frac{m}{l_1}\pi x) \sin(\frac{n}{l_2}\pi y)$. No such formulas exist for the other boundary conditions. To find the eigenvalues of (3) under the partially clamped conditions (6) we apply the rule of separation of variables. Chien, Chang and Mei in [5] have computed the eigenvalues by this method when $L = \partial^2/\partial x^2$ (the plate is compressed along its two sides). We will do the same procedure for $L = \Delta$.

Assume $w(x, y) = u(x)v(y) \neq 0$. Substituting the last expression into (3) one gets

$$D(u''''v + 2u''v'' + uv'''') + \lambda(u''v + uv'') = 0 \tag{39}$$

with boundary conditions

$$u(0) = u(l_1) = 0\,, \quad u'(0) = u'(l_1) = 0\,,$$

$$v(0) = v(l_2) = 0\,, \quad v''(0) = v''(l_2) = 0\,.$$

Choosing the basis $\sin\left(\frac{n}{l_2}\pi y\right) : n \in N$ for the space of functions

$$\left\{v \in C^4[0, l_2] : v(0) = v(l_2) = v''(0) = v''(l_2) = 0\right\}\,,$$

we reduce (39) to the fourth order ordinary differential equation

$$u'''' + \left(\lambda/D - 2(\pi n/l_2)^2\right)u'' + \left((\pi n/l_2)^4 - \lambda/D(\pi n/l_2)^2\right)u = 0 \tag{40}$$

with boundary conditions

$$u(0) = u(l_1) = 0,\ u'(0) = u'(l_1) = 0. \tag{41}$$

A general solution of the equation (40) is

$$u(x) = c_1 e^{\alpha_1 x} + c_2 e^{-\alpha_1 x} + c_3 \cos(\alpha_2 x) + c_4 \sin(\alpha_2 x),$$

where $\alpha_1 = \pi n/l_2$, $\alpha_2 = \sqrt{\lambda/D - (\pi n/l_2)^2}$ $\left(\lambda/D > (\pi n/l_2)^2\right)$. Hence, using the boundary conditions (41) we obtain

$$c_1 = -\frac{1}{2}\left(c_3 + \frac{\alpha_2}{\alpha_1}c_4\right),\ c_2 = \frac{1}{2}\left(\frac{\alpha_2}{\alpha_1}c_4 - c_3\right)$$

Table 1 All parameters equal unity (a polygonal plate)

(43)	(44) ($N = 30$)
37.800	52.345
58.470	92.126
85.081	92.126
104.289	128.215
105.119	154.130
147.291	167.031
156.250	189.583
171.728	189.583
173.456	246.327
211.797	246.327

Table 2 $E = 2 \cdot 10^5$, $h_0 = 1$, $l_1 = l_2 = 100$, $\nu = 0.17$ (a ferroconcrete plate)

(43)	(44) ($N = 30$)
518.994	718.708
802.797	1,264.904
1,168.173	1,264.904
1,431.901	1,760.406
1,443.298	2,116.224
2,022.322	2,293.361
2,145.335	2,602.998
2,381.570	2,602.998
2,930.948	3,382.105
3,335.552	3,382.105

and a system with respect to c_3 and c_4,

$$\begin{aligned}(\cos\alpha_2 l_1 - \cosh\alpha_1 l_1)c_3 + (\sin\alpha_2 l_1 - \frac{\alpha_2}{\alpha_1}\sinh\alpha_1 l_1)c_4 = 0,\\ -(\alpha_2\sin\alpha_2 l_1 + \alpha_1\sinh\alpha_1 l_1)c_3 + \alpha_2(\cos\alpha_2 l_1 - \cosh\alpha_1 l_1)c_4 = 0.\end{aligned} \tag{42}$$

The system (42) has a nontrivial solution if the determinant of the coefficients equals zero, i.e.,

$$\begin{aligned}2\alpha_2 + e^{\alpha_1 l_1}\left[\left(\alpha_1 - \frac{\lambda}{2\alpha_1 D}\right)\sin(\alpha_2 l_1) - \alpha_2\cos(\alpha_2 l_1)\right]\\ - e^{-\alpha_1 l_1}\left[\left(\alpha_1 - \frac{\lambda}{2\alpha_1 D}\right)\sin(\alpha_2 l_1) + \alpha_2\cos(\alpha_2 l_1)\right] = 0\,.\end{aligned} \tag{43}$$

We compute the eigenvalues of (3), (6) by solving the last equation (43) with respect to λ. Note that we can also solve the corresponding discrete problem for (3), (6). But it does not seem so convenient as the rule of separation.

To calculate eigenvalues of (3) under the totally clamped conditions (7) we solve the appropriate discretized linear problem (see (15)),

$$(\mathbf{K_1 w_N})_{mn} = \lambda(\mathbf{B w_N})_{mn}, \quad m, n = 1, 2, \ldots, N\,, \tag{44}$$

where $(\mathbf{K_1 w_N})_{mn}$ and $(\mathbf{B w_N})_{mn}$ are difference expressions defined in Subsection 3.2 (formulae (20–21)). The scheme (44) has the nine-point stencil and it is split into four independent subsystems, subjected to evenness of indexes (m, n). Each of these subsystems can be solved separately.[2]

Example 4.1 For $L = \Delta$ the first 10 eigenvalues λ for the partially and totally clamped plates with different properties, computed by (43) and (44) respectively, are given in Tables 1, 2:

[2]The algorithm has been implemented in `Numerical Python` code with the use of `LinearAlgebra.py` module of the `Python` library and the built-in `Cholesky_decomposition`.

5 The iterative method and numerical continuation algorithm

5.1 The iterative scheme

In this section we introduce the iterative scheme for solving (14). It is a combination of the Newton and the numerical continuation algorithm with respect to the load parameter λ. An alternative is to fix λ and vary the plate dimensions.

Let η be an eigenvalue of the linearized equation (3). Consider the segment $[\lambda_1, \lambda_1 + \Lambda]$, where $\lambda_1 = \eta + \varepsilon$, ε is a small positive number and Λ is an arbitrary positive number. Suppose $\lambda_{k+1} = \lambda_k + \delta_k$, $k = 1, 2 \ldots, M-1, \lambda_M = \lambda_1 + \Lambda$. To start Newton's iterations for the system of nonlinear algebraic equations (14) we choose $\lambda = \lambda_1$, then use the results for the next λ_2 and continue and so on. The Newton scheme for (14) after substitution of (14_2) into (14_1) is written down as

$$\overset{(\gamma+1)}{\mathbf{w_N}} = \overset{(\gamma)}{\mathbf{w_N}} - \mathbf{F}^{-1}_{\mathbf{w_N}}(\overset{(\gamma)}{\mathbf{w_N}}, \lambda_k)\mathbf{F}(\overset{(\gamma)}{\mathbf{w_N}}, \lambda_k), \quad \gamma = 0, 1, \ldots, \gamma_k - 1,$$

where

$$\mathbf{F} = \mathbf{K_1 w_N} - \mathbf{A_{1,N}}\left(\mathbf{w_N}, \mathbf{K_2}^{-1}\mathbf{A_{2,N}}(\mathbf{w_N}, \mathbf{w_N})\right) - \lambda \mathbf{B w_N},$$

$\mathbf{F} = (F^{11}, \ldots, F^{1N}, F^{21}, \ldots, F^{2N}, \ldots, F^{N1}, \ldots, F^{NN})^T$ and $\mathbf{F_{w_N}}$ is the Jacobian.

We can also apply a hybrid method. If the hybrid scheme with the application of the Gauss–Seidel and the Newton methods for outer and for inner iterations respectively, is used then

$$\overset{(\gamma+1)}{w_N^{mn}} = \overset{(\gamma)}{w_N^{mn}} - (F^{mn}_{w_N^{mn}})^{-1}\left(\overset{(\gamma+1)}{w_N^{11}}, \overset{(\gamma+1)}{w_N^{12}}, \ldots, \overset{(\gamma+1)}{w_N^{m,n-1}}, \overset{(\gamma)}{w_N^{mn}}, \ldots, \overset{(\gamma)}{w_N^{NN}}\right)$$

$$\times F^{mn}\left(\overset{(\gamma+1)}{w_N^{11}}, \overset{(\gamma+1)}{w_N^{12}}, \ldots, \overset{(\gamma+1)}{w_N^{m,n-1}}, \overset{(\gamma)}{w_N^{mn}}, \ldots, \overset{(\gamma)}{w_N^{NN}}\right),$$

$$\gamma = 0, 1, \ldots, \gamma_k - 1, \quad m, n = 1, 2, \ldots, N. \tag{45}$$

Below we demonstrate the effective algorithm for tracing branches of the solution which has been first introduced for calculating eigenfunctions for the totally clamped plate in [14]. It works as well for the other states of the plate.

Table 3 Coefficients w^{ij} and ψ^{ij}

i,j	1	3	i,j	1	3
1	0.288624	0.000313	1	−0.044862	0.001298
3	0.000313	0.000056	3	0.001298	0.000335

Table 4 Coefficients w^{ij}

i,j	1	3	5	7	9
1	0.288392				
3	0.000310	$5.6 \cdot 10^{-5}$		Sym. data	
5	$1.0 \cdot 10^{-5}$	$6.3 \cdot 10^{-6}$	$8.5 \cdot 10^{-7}$		
7	$1.8 \cdot 10^{-6}$	$1.5 \cdot 10^{-6}$	$2.7 \cdot 10^{-7}$	$1.1 \cdot 10^{-7}$	
9	$5.0 \cdot 10^{-7}$	$4.9 \cdot 10^{-7}$	$1.0 \cdot 10^{-7}$	$4.7 \cdot 10^{-8}$	$2.3 \cdot 10^{-8}$

5.2 The algorithm

Step 1. Start with $\lambda = \lambda_k = \eta + \varepsilon$, where $k = 1$.

Step 2. Choose the initial approximations $\overset{(0)}{w}{}_N^{ij}(\lambda_k)$ for the coefficients $w_N^{ij}(\lambda_k)$ in the expansion (8) by putting $\overset{(0)}{w}{}_N^{i_1 j_1}(\lambda_k) = c(\varepsilon) \neq 0$, $\overset{(0)}{w}{}_N^{ij}(\lambda_k) = 0$, $i \neq i_1$, $j \neq j_1$. Here $w_N^{i_1, j_1}$ is the largest coefficient in the expansion (8).

Step 3. Solve (14) by the Newton method with the initial approximations which have been chosen at Step 2. If the iterative process approaches the trivial solution or diverges then increase or decrease $|c(\varepsilon)|$, respectively, and return to Step 2.

Step 4. Put $\lambda = \lambda_{k+1} = \lambda_k + \delta_k$, where δ_k is a positive number.

Step 5. Choose the initial approximations $\overset{(0)}{w}{}_N^{ij}(\lambda_{k+1})$ by putting $\overset{(0)}{w}{}_N^{ij}(\lambda_{k+1}) = \overset{(\gamma_k)}{w}{}_N^{ij}(\lambda_k)$, $i, j = 1, 2, \ldots, N$.

Step 6. Solve (14) by the Newton method with the initial approximations which have been chosen at Step 5. If the process diverges or approaches the trivial solution then decrease δ_k and return to Step 4.

Step 7. Repeat Steps 4, 5, 6 for $k = 2, 3 \ldots, M - 1$ until $\lambda = \lambda_M = \lambda_1 + \Lambda$.

In the algorithm the largest coefficient $w_N^{i_1 j_1}$ can be revealed by solving the linearized equation (3). For instance, for the first eigenvalue $\eta = 718.708$ (see Table 2 in the example of Section 4) the largest component of the corresponding eigenvector is w_N^{11}. Therefore in the algorithm we should put $\overset{(0)}{w}{}_N^{11}(\lambda_k) = c(\varepsilon) \neq 0$.

If the solution jumps on the other branch at Step 6 then we deal with the secondary bifurcation or mode jumping. The secondary bifurcation points can be also found by monitoring the determinant of the augmented tangent matrix [3]. It is the classical Euler–Newton approach. Chien, Chang and Mei [5] suggest monitoring the condition number of the reduced matrix. One of the effective approaches is described in Dossou and Pierre's work [10]. Singular points, where the determinant

Table 5 Coefficients ψ^{ij}

i,j	1	3	5	7	9
1	−0.044788				
3	0.001297	0.000335		Sym. data	
5	$6.9 \cdot 10^{-5}$	$4.7 \cdot 10^{-5}$	$1.1 \cdot 10^{-5}$		
7	$1.2 \cdot 10^{-5}$	$1.1 \cdot 10^{-5}$	$3.3 \cdot 10^{-6}$	$1.3 \cdot 10^{-6}$	
9	$3.2 \cdot 10^{-6}$	$3.6 \cdot 10^{-6}$	$1.2 \cdot 10^{-6}$	$5.6 \cdot 10^{-7}$	$2.7 \cdot 10^{-7}$

of the Jacobian vanishes can be detected along solution curves by a scalar quantity (detector). This scalar quantity changes sign at the same points on the curves as the determinant of the Jacobian matrix. The same idea has been applied in [11].

6 Numerical experiments

Here we demonstrate numerical results of solving the problem (2) ($L = \Delta$) by the above described techniques. The computed Fourier coefficients in the expansion (8) for the first three branches of the solution for a polygonal square ($l_1 = l_2 = 1$) simply supported plate are presented by tables. To decrease the volume of computations one can first apply the procedure for small N and then use the obtained data as initial approximations for calculations with larger N. Suppose $z = \max\limits_{1\le i,\, j\le N} \left| w_N^{ij(\gamma_k)} - w_N^{ij(\gamma_k-1)} \right|$. Further, let $G_M = \{(x_m, y_n), m, n = 1, 2, \ldots, 10\}$ and γ be a number of iterations.

Example 6.1 (Tables 3, 4, 5, 6, and 7) $\lambda = \lambda_{11} + \varepsilon = 20.239$ ($\varepsilon = 0.5$); the initial approximation: $w_N^{11(0)} = 0.288$, $w_N^{ij(0)} = 0$, $i, j \ne 1$.

In this example $w_N^{ij} = 0$ and $\psi_N^{ij} = 0$ for even i, j. Further, in Table 3: $N = 3$, $\gamma = 4$, $z = 8.9 \cdot 10^{-8}$; in Tables 4, 5: $N = 9$, $\gamma = 4$, $z = 1.8 \cdot 10^{-6}$; and in Tables 6, 7: $N = 15$, $\gamma = 3$, $z = 8.2 \cdot 10^{-6}$.

For the deflection and the stress function we have

$$\begin{aligned} \max_{G_M} |W_3(x_i, y_j) - W_9(x_i, y_j)| &= 4.4 \cdot 10^{-4}, \\ \max_{G_M} |\Psi_3(x_i, y_j) - \Psi_9(x_i, y_j)| &= 3.3 \cdot 10^{-4}, \end{aligned} \tag{46}$$

$$\begin{aligned} \max_{G_M} |W_9(x_i, y_j) - W_{15}(x_i, y_j)| &= 6.4 \cdot 10^{-6}, \\ \max_{G_M} |\Psi_9(x_i, y_j) - \Psi_{15}(x_i, y_j)| &= 7.9 \cdot 10^{-6}. \end{aligned} \tag{47}$$

Example 6.2 (Tables 8, 9, 10, 11, and 12) $\lambda = \lambda_{12} + \varepsilon = 49.848$; $w_N^{12(0)} = 0.181$, $w_N^{ij(0)} = 0$, $i \ne 1$, $j \ne 2$; $w^{ij} = 0$ for even i and odd j; $\psi^{ij} = 0$ for even i, j.

In Table 8: $N = 4$, $\gamma = 3$, $z = 1.6 \cdot 10^{-6}$; in Tables 9, 10: $N = 10$, $\gamma = 3$; $z = 1.5 \cdot 10^{-6}$ and in Tables 11, 12: $N = 16$, $\gamma = 3$, $z = 6.0 \cdot 10^{-6}$.

For the deflection and the stess function we have

$$\begin{aligned} \max_{G_M} |W_4(x_i, y_j) - W_{10}(x_i, y_j)| &= 2.0 \cdot 10^{-3}, \\ \max_{G_M} |\Psi_4(x_i, y_j) - \Psi_{10}(x_i, y_j)| &= 1.7 \cdot 10^{-3}, \end{aligned} \tag{48}$$

Table 6 Coefficients w^{ij}

i,j	1	3	5	7	9	11	13	15
1	0.288389							
3	0.000310	$5.6 \cdot 10^{-5}$		Sym. data				
5	$1.0 \cdot 10^{-5}$	$6.3 \cdot 10^{-6}$	$8.5 \cdot 10^{-7}$					
7	$1.8 \cdot 10^{-6}$	$1.5 \cdot 10^{-6}$	$2.7 \cdot 10^{-7}$	$1.1 \cdot 10^{-7}$				
9	$5.0 \cdot 10^{-7}$	$4.9 \cdot 10^{-7}$	$1.1 \cdot 10^{-7}$	$4.8 \cdot 10^{-8}$	$2.4 \cdot 10^{-8}$			
11	$1.8 \cdot 10^{-7}$	$1.9 \cdot 10^{-7}$	$4.6 \cdot 10^{-8}$	$2.3 \cdot 10^{-8}$	$1.3 \cdot 10^{-8}$	$7.3 \cdot 10^{-9}$		
13	$7.8 \cdot 10^{-8}$	$8.6 \cdot 10^{-8}$	$2.2 \cdot 10^{-8}$	$1.2 \cdot 10^{-8}$	$7.1 \cdot 10^{-9}$	$4.3 \cdot 10^{-9}$	$2.7 \cdot 10^{-9}$	
15	$3.8 \cdot 10^{-8}$	$4.3 \cdot 10^{-8}$	$1.2 \cdot 10^{-8}$	$6.6 \cdot 10^{-9}$	$4.1 \cdot 10^{-9}$	$2.6 \cdot 10^{-9}$	$1.7 \cdot 10^{-9}$	$1.1 \cdot 10^{-9}$

Table 7 Coefficients ψ^{ij}

i,j	1	3	5	7	9	11	13	15
1	-0.044787							
3	0.001297	0.000335		Sym. data				
5	$6.9 \cdot 10^{-5}$	$4.7 \cdot 10^{-5}$	$1.1 \cdot 10^{-5}$					
7	$1.2 \cdot 10^{-5}$	$1.1 \cdot 10^{-5}$	$3.3 \cdot 10^{-6}$	$1.3 \cdot 10^{-6}$				
9	$3.2 \cdot 10^{-6}$	$3.6 \cdot 10^{-6}$	$1.2 \cdot 10^{-6}$	$5.6 \cdot 10^{-7}$	$2.7 \cdot 10^{-7}$			
11	$1.2 \cdot 10^{-6}$	$1.4 \cdot 10^{-6}$	$5.3 \cdot 10^{-7}$	$2.6 \cdot 10^{-7}$	$1.4 \cdot 10^{-7}$	$8.1 \cdot 10^{-8}$		
13	$5.0 \cdot 10^{-7}$	$6.2 \cdot 10^{-7}$	$2.5 \cdot 10^{-7}$	$1.4 \cdot 10^{-7}$	$7.9 \cdot 10^{-8}$	$4.8 \cdot 10^{-8}$	$3.0 \cdot 10^{-8}$	
15	$2.4 \cdot 10^{-7}$	$3.1 \cdot 10^{-7}$	$1.3 \cdot 10^{-7}$	$7.4 \cdot 10^{-8}$	$4.5 \cdot 10^{-8}$	$2.9 \cdot 10^{-8}$	$1.9 \cdot 10^{-8}$	$1.1 \cdot 10^{-8}$

Table 8 Coefficients w^{ij} and ψ^{ij}

i,j	2	4	i,j	1	3
1	0.180865	0.000119	1	−0.042327	−0.002286
3	0.000313	0.000026	3	0.002413	0.000066

$$\max_{G_M} |W_{10}(x_i, y_j) - W_{16}(x_i, y_j)| = 1.0 \cdot 10^{-5},$$
$$\max_{G_M} |\Psi_{10}(x_i, y_j) - \Psi_{16}(x_i, y_j)| = 1.2 \cdot 10^{-5}. \quad (49)$$

Example 6.3 (Tables 13, 14, 15, 16, and 17) $\lambda = \lambda_{22} + \varepsilon = 79.457$; $\overset{(0)}{w}{}^{22}_{N} = 0.131$, $\overset{(0)}{w}{}^{ij}_{N} = 0$, $i, j \neq 2$; $w^{ij} = 0$ for odd i, j and $\psi^{ij} = 0$ for even i, j.

In Table 13: $N = 4$, $\gamma = 3$, $z = 3.0 \cdot 10^{-8}$; in Tables 14, 15: $N = 10$, $\gamma = 3$, $z = 2.7 \cdot 10^{-6}$ and in Tables 16, 17: $N = 16$, $\gamma = 3$, $z = 4.8 \cdot 10^{-7}$.

For the deflection and the stess function we have

$$\max_{G_M} |W_4(x_i, y_j) - W_{10}(x_i, y_j)| = 1.2 \cdot 10^{-2},$$
$$\max_{G_M} |\Psi_4(x_i, y_j) - \Psi_{10}(x_i, y_j)| = 6.6 \cdot 10^{-3}, \quad (50)$$

$$\max_{G_M} |W_{10}(x_i, y_j) - W_{16}(x_i, y_j)| = 3.4 \cdot 10^{-5},$$
$$\max_{G_M} |\Psi_{10}(x_i, y_j) - \Psi_{16}(x_i, y_j)| = 2.7 \cdot 10^{-5}. \quad (51)$$

Table 9 Coefficients w^{ij}

i,j	2	4	6	8	10
1	0.179786	0.000121	$1.2 \cdot 10^{-5}$	$1.7 \cdot 10^{-6}$	$5.0 \cdot 10^{-7}$
3	0.000302	$2.6 \cdot 10^{-5}$	$5.8 \cdot 10^{-6}$	$1.3 \cdot 10^{-6}$	$4.4 \cdot 10^{-7}$
5	$3.3 \cdot 10^{-6}$	$4.1 \cdot 10^{-6}$	$1.3 \cdot 10^{-6}$	$2.5 \cdot 10^{-7}$	$9.9 \cdot 10^{-8}$
7	$8.1 \cdot 10^{-7}$	$1.1 \cdot 10^{-6}$	$4.6 \cdot 10^{-7}$	$1.1 \cdot 10^{-7}$	$4.8 \cdot 10^{-8}$
9	$2.7 \cdot 10^{-7}$	$3.7 \cdot 10^{-7}$	$1.9 \cdot 10^{-7}$	$4.9 \cdot 10^{-8}$	$2.5 \cdot 10^{-8}$

Table 10 Coefficients ψ^{ij}

i,j	1	3	5	7	9
1	−0.041822	−0.002259	0.000301	$2.8 \cdot 10^{-5}$	$6.3 \cdot 10^{-6}$
3	0.002386	$6.6 \cdot 10^{-5}$	0.000112	$2.0 \cdot 10^{-5}$	$5.9 \cdot 10^{-6}$
5	0.000143	$-1.6 \cdot 10^{-6}$	$2.7 \cdot 10^{-5}$	$6.0 \cdot 10^{-6}$	$2.1 \cdot 10^{-6}$
7	$2.5 \cdot 10^{-5}$	$-1.1 \cdot 10^{-6}$	$8.5 \cdot 10^{-6}$	$2.3 \cdot 10^{-6}$	$9.4 \cdot 10^{-7}$
9	$6.9 \cdot 10^{-6}$	$-4.4 \cdot 10^{-7}$	$3.2 \cdot 10^{-6}$	$1.0 \cdot 10^{-6}$	$4.6 \cdot 10^{-7}$

Table 11 Coefficients w^{ij}

i,j	2	4	6	8	10	12	14	16
1	0.179780	0.000121	$1.2 \cdot 10^{-5}$	$1.7 \cdot 10^{-6}$	$5.0 \cdot 10^{-7}$	$1.9 \cdot 10^{-7}$	$8.5 \cdot 10^{-8}$	$4.2 \cdot 10^{-8}$
3	0.000302	$2.6 \cdot 10^{-5}$	$5.8 \cdot 10^{-6}$	$1.3 \cdot 10^{-6}$	$4.4 \cdot 10^{-7}$	$1.9 \cdot 10^{-7}$	$8.8 \cdot 10^{-8}$	$4.6 \cdot 10^{-8}$
5	$3.3 \cdot 10^{-6}$	$4.1 \cdot 10^{-6}$	$1.3 \cdot 10^{-6}$	$2.5 \cdot 10^{-7}$	$1.0 \cdot 10^{-7}$	$4.5 \cdot 10^{-8}$	$2.2 \cdot 10^{-8}$	$1.2 \cdot 10^{-8}$
7	$8.0 \cdot 10^{-7}$	$1.1 \cdot 10^{-6}$	$4.6 \cdot 10^{-7}$	$1.1 \cdot 10^{-7}$	$4.9 \cdot 10^{-8}$	$2.4 \cdot 10^{-8}$	$1.3 \cdot 10^{-8}$	$7.2 \cdot 10^{-9}$
9	$2.6 \cdot 10^{-7}$	$3.7 \cdot 10^{-7}$	$1.9 \cdot 10^{-7}$	$5.2 \cdot 10^{-8}$	$2.6 \cdot 10^{-8}$	$1.4 \cdot 10^{-8}$	$7.7 \cdot 10^{-9}$	$4.6 \cdot 10^{-9}$
11	$9.9 \cdot 10^{-8}$	$1.5 \cdot 10^{-7}$	$8.3 \cdot 10^{-8}$	$2.6 \cdot 10^{-8}$	$1.4 \cdot 10^{-8}$	$8.0 \cdot 10^{-9}$	$4.8 \cdot 10^{-9}$	$3.0 \cdot 10^{-9}$
13	$4.4 \cdot 10^{-8}$	$6.9 \cdot 10^{-8}$	$4.1 \cdot 10^{-8}$	$1.4 \cdot 10^{-8}$	$8.1 \cdot 10^{-9}$	$4.9 \cdot 10^{-9}$	$3.0 \cdot 10^{-9}$	$2.0 \cdot 10^{-9}$
15	$2.2 \cdot 10^{-8}$	$3.5 \cdot 10^{-8}$	$2.2 \cdot 10^{-8}$	$7.8 \cdot 10^{-9}$	$4.8 \cdot 10^{-9}$	$3.0 \cdot 10^{-9}$	$2.0 \cdot 10^{-9}$	$1.3 \cdot 10^{-9}$

Table 12 Coefficients ψ^{ij}

i,j	1	3	5	7	9	11	13	15
1	−0.041819	−0.002258	0.000301	$2.8 \cdot 10^{-5}$	$6.3 \cdot 10^{-6}$	$2.1 \cdot 10^{-6}$	$8.6 \cdot 10^{-7}$	$4.1 \cdot 10^{-7}$
3	0.002385	$6.6 \cdot 10^{-5}$	$1.1 \cdot 10^{-4}$	$2.0 \cdot 10^{-5}$	$5.9 \cdot 10^{-6}$	$2.2 \cdot 10^{-6}$	$9.9 \cdot 10^{-7}$	$4.9 \cdot 10^{-7}$
5	$1.4 \cdot 10^{-4}$	$-1.6 \cdot 10^{-6}$	$2.7 \cdot 10^{-5}$	$6.0 \cdot 10^{-6}$	$2.1 \cdot 10^{-6}$	$8.6 \cdot 10^{-7}$	$4.0 \cdot 10^{-7}$	$2.1 \cdot 10^{-7}$
7	$2.5 \cdot 10^{-5}$	$-1.1 \cdot 10^{-6}$	$8.5 \cdot 10^{-6}$	$2.3 \cdot 10^{-6}$	$9.4 \cdot 10^{-7}$	$4.3 \cdot 10^{-7}$	$2.2 \cdot 10^{-7}$	$1.2 \cdot 10^{-7}$
9	$6.9 \cdot 10^{-6}$	$-4.3 \cdot 10^{-7}$	$3.2 \cdot 10^{-6}$	$1.0 \cdot 10^{-6}$	$4.6 \cdot 10^{-7}$	$2.3 \cdot 10^{-7}$	$1.3 \cdot 10^{-7}$	$7.2 \cdot 10^{-8}$
11	$2.5 \cdot 10^{-6}$	$-1.8 \cdot 10^{-7}$	$1.4 \cdot 10^{-6}$	$4.8 \cdot 10^{-7}$	$2.4 \cdot 10^{-7}$	$1.3 \cdot 10^{-7}$	$7.6 \cdot 10^{-8}$	$4.6 \cdot 10^{-8}$
13	$1.1 \cdot 10^{-6}$	$-8.7 \cdot 10^{-8}$	$6.6 \cdot 10^{-7}$	$2.5 \cdot 10^{-7}$	$1.3 \cdot 10^{-7}$	$7.8 \cdot 10^{-8}$	$4.8 \cdot 10^{-8}$	$3.0 \cdot 10^{-8}$
15	$5.3 \cdot 10^{-7}$	$-4.5 \cdot 10^{-8}$	$3.4 \cdot 10^{-7}$	$1.4 \cdot 10^{-7}$	$7.7 \cdot 10^{-8}$	$4.7 \cdot 10^{-8}$	$3.1 \cdot 10^{-8}$	$1.9 \cdot 10^{-8}$

Table 13 Coefficients w^{ij} and ψ^{ij}

i,j	2	4	i,j	1	3
2	0.131129	0.000023	1	−0.029717	0.004021
4	0.000023	0.000022	3	0.004021	0.000788

In Tables 3, 4, 5, 6, 7, 8, 9, 10, 11, 12, 13, 14, 15, 16, and 17 for simplicity we use the notations $w^{ij} \equiv \overset{(\gamma)}{w}{}^{ij}_{N}$, $\psi^{ij} \equiv \overset{(\gamma)}{\psi}{}^{ij}_{N}$.

From the above given examples we can see that the Fourier coefficients are decreasing according to the estimates (24) (Lemma 3.1). Besides, a few iterations (with not large N) are needed to get high accuracy of approximation.

From Tables 3, 4, 5, 6, 7, 8, 9, 10, 11, 12, 13, 14, 15, 16, and 17 and the formulas (46–51) one can see that for $N = 3, 4$ and $N = 9, 10$, as minimum two and five digits of accuracy are achieved, respectively. Thus, theoretically established the rate of convergence for the Fourier coefficients (Lemma 3.2) and the error of approximation for the solution (Theorem 3.1) are observed in the above given numerical data i.e., the numerical experiments confirm the theoretical results.

The computations have been also done for the ferroconcrete simply supported plate with $E = 2 \cdot 10^{-5}$, $\nu = 0.17$, $h_0 = 1$. Figures 1, 2, 3, and 4 show the bifurcation scenario for the deflection W_N. On Figs. 1, 3 ω_{ij} denote that basis function which has the largest weight in the expansion (8) for $W_N(x, y)$. On Fig. 1 $\max\limits_{G_M} W_N(x_i, y_j)$ and $\min\limits_{G_M} W_N(x_i, y_j)$ of the first two curves of the solution W_N (Branches I, II) and their symmetrical ones are sketched. The bifurcation point η_2 is double and we choose $\overset{(0)}{w}{}^{12}_{N}(\eta_2 + \varepsilon) \neq 0$ or $\overset{(0)}{w}{}^{21}_{N}(\eta_2 + \varepsilon) \neq 0$. The contours of the solution branches are shown on Fig. 2. Figure 3 demonstrates the effect of appearance of the secondary bifurcation point $\eta = 783.810$. This results from splitting the double bifurcation point

Table 14 Coefficients w^{ij}

i,j	2	4	6	8	10
2	0.124582				
4	$4.3 \cdot 10^{-5}$	$1.5 \cdot 10^{-5}$		Sym. data	
6	$1.9 \cdot 10^{-5}$	$4.4 \cdot 10^{-6}$	$2.2 \cdot 10^{-6}$		
8	$1.3 \cdot 10^{-6}$	$8.3 \cdot 10^{-7}$	$5.9 \cdot 10^{-7}$	$1.2 \cdot 10^{-7}$	
10	$4.0 \cdot 10^{-7}$	$3.0 \cdot 10^{-7}$	$2.4 \cdot 10^{-7}$	$6.0 \cdot 10^{-8}$	$3.2 \cdot 10^{-8}$

Table 15 Coefficients ψ^{ij}

i,j	1	3	5	7	9
1	−0.026812				
3	−0.003629	−0.000712		Sym. data	
5	$6.4 \cdot 10^{-4}$	$6.9 \cdot 10^{-5}$	$7.2 \cdot 10^{-5}$		
7	$6.5 \cdot 10^{-5}$	$2.3 \cdot 10^{-6}$	$1.8 \cdot 10^{-5}$	$5.1 \cdot 10^{-6}$	
9	$1.6 \cdot 10^{-5}$	$-1.2 \cdot 10^{-7}$	$6.4 \cdot 10^{-6}$	$2.1 \cdot 10^{-6}$	$9.6 \cdot 10^{-7}$

Table 16 Coefficients w^{ij}

i,j	2	4	6	8	10	12	14	16
2	0.124564							
4	$4.3 \cdot 10^{-5}$	$1.5 \cdot 10^{-5}$		Sym. data				
6	$1.9 \cdot 10^{-5}$	$4.4 \cdot 10^{-6}$	$2.2 \cdot 10^{-6}$					
8	$1.3 \cdot 10^{-6}$	$8.4 \cdot 10^{-7}$	$5.9 \cdot 10^{-7}$	$1.3 \cdot 10^{-7}$				
10	$4.0 \cdot 10^{-7}$	$3.0 \cdot 10^{-7}$	$2.5 \cdot 10^{-7}$	$6.2 \cdot 10^{-8}$	$3.2 \cdot 10^{-8}$			
12	$1.6 \cdot 10^{-7}$	$1.3 \cdot 10^{-7}$	$1.2 \cdot 10^{-7}$	$3.2 \cdot 10^{-8}$	$1.8 \cdot 10^{-8}$	$1.0 \cdot 10^{-8}$		
14	$7.2 \cdot 10^{-8}$	$6.2 \cdot 10^{-8}$	$6.0 \cdot 10^{-8}$	$1.7 \cdot 10^{-8}$	$1.0 \cdot 10^{-8}$	$6.2 \cdot 10^{-9}$	$3.9 \cdot 10^{-9}$	
16	$3.6 \cdot 10^{-8}$	$3.3 \cdot 10^{-8}$	$3.2 \cdot 10^{-8}$	$1.0 \cdot 10^{-8}$	$6.2 \cdot 10^{-9}$	$4.0 \cdot 10^{-9}$	$2.6 \cdot 10^{-9}$	$1.8 \cdot 10^{-9}$

Table 17 Coefficients ψ^{ij}

i,j	1	3	5	7	9	11	13	15
1	-0.026804							
3	-0.003628	-0.000711		Sym. data				
5	0.000644	$6.9 \cdot 10^{-5}$	$7.2 \cdot 10^{-5}$					
7	$6.5 \cdot 10^{-5}$	$2.3 \cdot 10^{-6}$	$1.8 \cdot 10^{-5}$	$5.1 \cdot 10^{-6}$				
9	$1.6 \cdot 10^{-5}$	$-1.2 \cdot 10^{-7}$	$6.4 \cdot 10^{-6}$	$2.1 \cdot 10^{-6}$	$9.6 \cdot 10^{-7}$			
11	$5.4 \cdot 10^{-6}$	$-1.9 \cdot 10^{-7}$	$2.7 \cdot 10^{-6}$	$9.6 \cdot 10^{-7}$	$4.8 \cdot 10^{-7}$	$2.7 \cdot 10^{-7}$		
13	$2.2 \cdot 10^{-6}$	$-1.2 \cdot 10^{-7}$	$1.3 \cdot 10^{-6}$	$4.9 \cdot 10^{-7}$	$2.6 \cdot 10^{-7}$	$1.5 \cdot 10^{-7}$	$9.4 \cdot 10^{-8}$	
15	$1.1 \cdot 10^{-6}$	$-6.8 \cdot 10^{-8}$	$6.6 \cdot 10^{-7}$	$2.6 \cdot 10^{-7}$	$1.5 \cdot 10^{-7}$	$9.2 \cdot 10^{-8}$	$5.9 \cdot 10^{-8}$	$3.8 \cdot 10^{-8}$

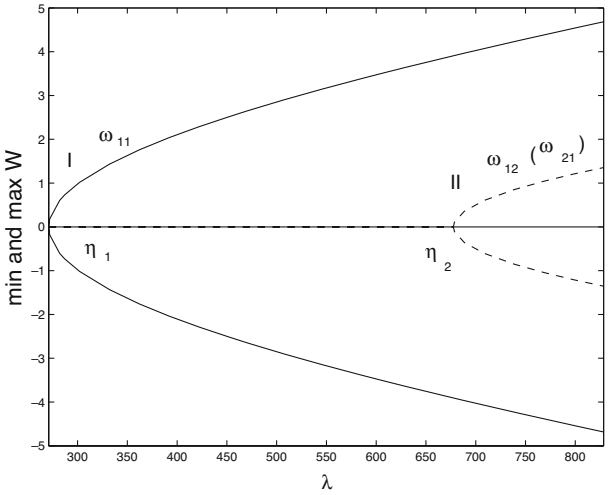

Fig. 1 $l_1 = l_2 = 100$, $N = 6$, $\eta_1 = \lambda_{11} = 271.022$, $\eta_2 = \lambda_{12} = \lambda_{21} = 677.555$

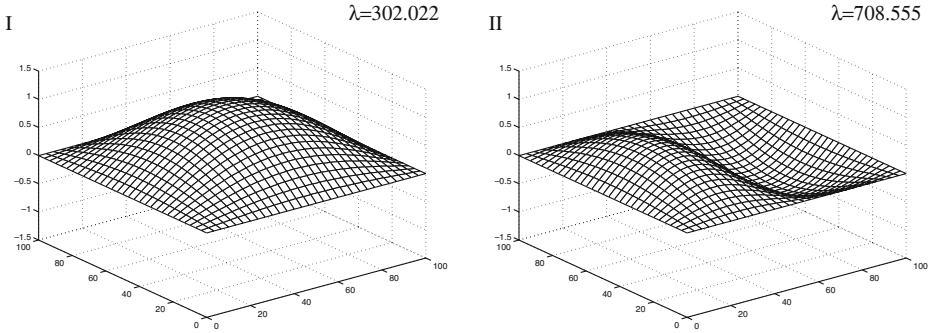

Fig. 2 The contours of the solution branches I, II in Fig. 1

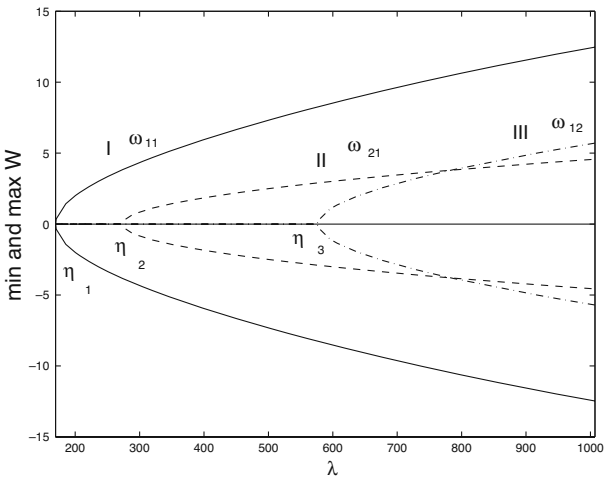

Fig. 3 $l_1 = 200, l_2 = 100$, $N = 6$, $\eta_1 = \lambda_{11} = 169.389$, $\eta_2 = \lambda_{21} = 271.022$, $\eta_3 = \lambda_{12} = 575.922$

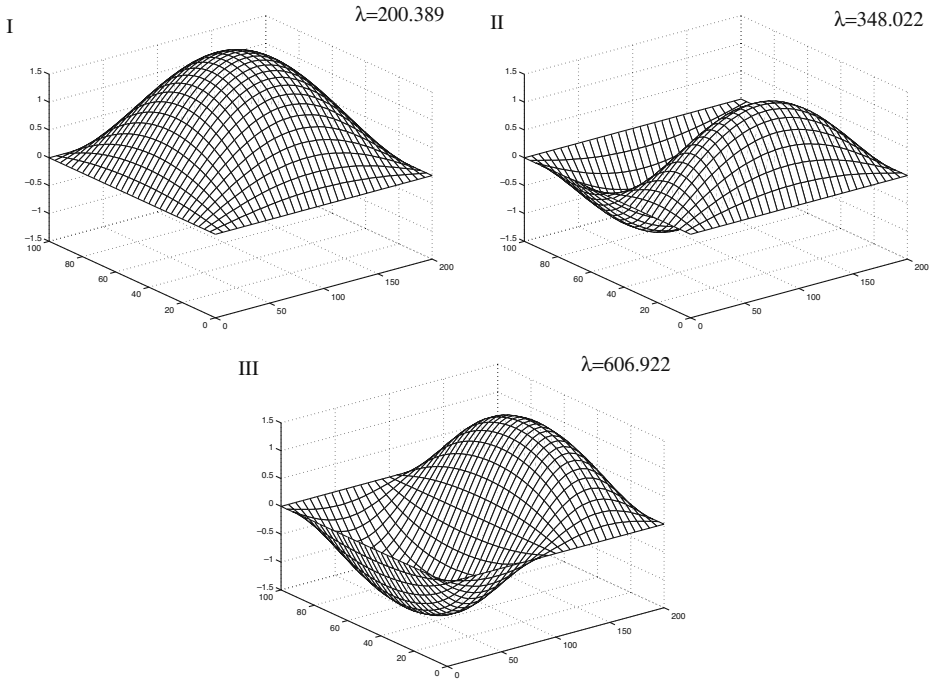

Fig. 4 The contours of the solution branches I, II, III in Fig. 3

by perturbation. On Fig. 4 the corresponding contours of the solution branches are shown. Note, monitoring the determinant of the augmented Jacobian matrix can not detect double bifurcation points [2]. Numerical methods for computing such bifurcation points can be found, e.g. in [7]. In that work the block and band Lanczos algorithms for computing multiple bifurcation points and the Ritz vectors for branch switching are suggested.

Acknowledgements I am grateful to Prof. Michael Osborne (the Australian National University) for his valuable suggestions, Dr. Kokou Dossou (University of Technology Sydney) who helped to improve my understanding of the subject, Assoc. Prof. George Stavroulakis (University of Ioannina) and Prof. Tamaz Vashakmadze (the Tbilisi State University) for their interest in this work. I also wish to thank the anonymous referees for their careful reading of the manuscript and their fruitful comments.

References

1. Adams, R.A.: Sobolev Spaces. Academic, New York, San Francisko, London (1975)
2. Allgower, E.L., Chien, C.S.: Continuation and local perturbation for multiple bifurcations. SIAM J. Sci. Comput. **7**, 1265–1281 (1986)
3. Allgower, E.L., Georg, K.: Numerical Continuation Methods. Springer, Berlin (1990)
4. Caloz, G., Rappaz, J.: Numerical analysis for nonlinear and bifurcation problems. Handbook of numerical analysis, North Holland, Amsterdam, vol. **V**, pp. 487–637 (1997)

5. Chien, C.S., Chang, S.L., Mei, Z.: Tracing the buckling of a rectangular plate with the Block GMRES method. J. Comput. Appl. Math. **136**, 199–218 (2001) [Online] http://www.elsevier.com/locate/cam
6. Chien, C.S., Gong, S.Y., Mei, Z.: Mode jumping in the von Kármán equations. SIAM J. Sci. Comput. **22**(4), 1354–1385 (2000) [Online] http://epubs.siam.org/sam-bin/dbq/article/30732
7. Chien, C.S., Weng, Z.L., Shen, C.L.: Lanczos-type methods for continuation problems. Numer. Linear Algebra Appl. **4**, 23–41 (1997)
8. Ciarlet, P., Rabier, P.: Les equations de von ká. Springer-Verlag, Berlin Heidelberg, New York (1980)
9. Dossou, K.: Résolution numérique des équations de von Karman. Thèse, Department de mathématiques et de statistique. FacultTé des Sciences et Génie Université Laval Québeg (2000)
10. Dossou, K., Pierre, R.: A Newton-GMRES approach for the analysis of the postbuckling behavior of the solutions of the von Kármán equations. SIAM J. Sci. Comput. **24**(6), 1994–2012 (2003) [Online] http://epubs.siam.org/sam-bin/dbq/article/37614
11. Harrar, D.L., Osborne, M.R.: Computing eigenvalues of ordinary differential equations. ANZIAM J. **44**(E), C313–C334 (2003) [Online] http://anziamj.austms.org.au/V44/CTAC2001/Harr
12. Holder, E.J., Schaeffer, D.G.: Boundary conditions and mode jumping in the von Kármán's equations. SIAM J. Math. Anal. **15**, 446–458 (1984)
13. Keller, H.: Numerical solution of bifurcation and nonlinear eigenvalue problem. In: Rabinovitz, P.H. (ed.) Applications of Bifurcation Theory, pp. 359–384. Academic, New York (1977)
14. Muradova, A.D.: Numerical techniques for linear and nonlinear eigenvalue problems in the theory of elasticity. ANZIAM J. **46**(E), C426–C438 (2005) [Online] http://anziamj.austms.org.au/V46/CTAC2004/Mura
15. Schaeffer, D.G., Golubitsky, M.: Boundary conditions and mode jumping in the buckling of a rectangular plate. Comm. Math. Phys. **69**, 209–236 (1979)
16. Vashakmadze, T.S.: The Theory of Anisotropic Elastic Plates. Kluwer, Dordrecht, Boston, London (1999)